Subcellular dynamics of T cell immunological synapses and kinapses in lymph nodes

Georges A. Azar[a,b], Fabrice Lemaître[a,b], Ellen A. Robey[c], and Philippe Bousso[a,b,1]

[a]G5 Dynamiques des Réponses Immunes, Institut Pasteur, 75015 Paris, France; [b]Institut National de la Santé et de la Recherche Médicale U668, Equipe Avenir, 75015 Paris, France; and [c]Department of Molecular and Cell Biology, Life Sciences Addition, University of California, Berkeley, CA 94720

Edited by Michael L. Dustin, Skirball Institute of Biomolecular Medicine, New York, NY, and accepted by the Editorial Board January 8, 2010 (received for review May 28, 2009)

In vitro studies have revealed that T cell activation occurs during the formation of either dynamic or stable interactions with antigen-presenting cells (APC), and the respective cell junctions have been referred to as immunological kinapses and synapses. However, the relevance and molecular dynamics of kinapses and synapses remain to be established in vivo. Using two-photon imaging, we tracked the distribution of LAT-EGFP molecules during antigen recognition by activated CD4$^+$ T cells in lymph nodes. At steady state, LAT-EGFP molecules were preferentially found at the uropod of rapidly migrating T cells. In contrast to naïve T cells that fully stopped upon systemic antigen delivery, recently activated T cells decelerated and formed kinapses, characterized by continuous extension of membrane protrusions and by the absence of persistent LAT-EGFP clustering. On the other hand, activated CD4$^+$ T cells formed stable immunological synapses with antigen-loaded B cells and displayed sustained accumulation of LAT-EGFP fluorescence at the contact zone. Our results show that the state of T cell activation and the type of APC largely influence T cell–APC contact dynamics in lymph nodes. Furthermore, we provide a dynamic look at immunological kinapses and synapses in lymph nodes and suggest the existence of distinct patterns of LAT redistribution during antigen recognition.

T cell activation | two-photon imaging | LAT | B cells

T cell activation and functions are initiated during cellular interactions with antigen-presenting cells (APC). The molecular organization of the T cell–APC contact area, termed immunological synapse, has been studied extensively in various in vitro settings (reviewed in ref. 1). Reorganization of the actin cytoskeleton (2, 3), translocation of the microtubule organizing center (4, 5), segregation of surface and signaling molecules into central and peripheral regions of the contact zone (cSMAC and pSMAC, respectively) (6, 7), condensation of membrane microdomains (8), and formation of dynamic microclusters (9–13) contribute to immunological synapse formation and have been proposed to participate in and/or regulate T cell activation. Of note, the topology of the immunological synapse is not unique and may depend on the type of APC, the T cell phenotype, and the strength of stimulation (14–16). In various experimental conditions, both bull's eye shaped and multifocal synapses have been described (6, 7, 17, 18).

In sharp contrast, evidence for organized immunological synapse and cSMAC formation in vivo is scarce and has been limited to static images (19–23). This remains a critical issue because T cell and APC behaviors are profoundly dependent on their surrounding microenvironment. For instance, T cells are highly motile in secondary lymphoid organs (24) but largely sessile in cell suspension. Thus, the topology and dynamics of T cell synapses in vivo remain to be established (25).

Two-photon imaging is a technique of choice to tackle immune cell behavior in physiologic settings (26). Several studies have characterized the frequency, stability, and duration of interactions established by T cells and dendritic cells (DCs) or B cells in intact lymph nodes (reviewed in refs. 27 and 28). One of the interesting observations offered by these studies is that antigen (Ag) recognition by T cells can occur during long-lived interactions (lasting several hours) or during more dynamic and transient contacts (lasting a few minutes at most) with APCs. The term *kinapse* has been introduced recently to refer to such a dynamic mode of cellular interaction (29). In these imaging experiments, T cells were labeled with a cytoplasmic dye offering little insight into the subcellular dynamics underlying Ag recognition and more specifically into immunological synapse or kinapse formation. Tracking the distribution of fluorescently tagged molecules with two-photon imaging is technically challenging because of the relatively low signal-to-noise ratio when imaging in deep regions of lymph nodes.

The linker for T cell activation (LAT) protein acts as a critical scaffold during T cell activation (30). LAT is distributed at the plasma membrane in detergent-resistant membrane fractions (31, 32) and in intracellular compartments, and both pools are recruited to the cell junction in vitro (33). LAT seems to be essential for its own recruitment (33), could contribute to the condensation of membrane domains at the immunological synapse (34), and accumulates in microclusters (10). Therefore, LAT is a particularly interesting candidate molecule to assess the relevance of the immunological synapse in lymphoid organs.

In the present report, we show that T cells expressing a LAT-EGFP fusion molecule by retroviral transduction can be visualized in real time by two-photon imaging within intact lymph nodes. Using this approach, we report the dynamics of LAT-EGFP in T cells at steady state and during two modes of activation. Our results provide an initial glimpse at immunological synapse and kinapse dynamics in secondary lymphoid organs.

Results and Discussion

Recently Activated T Cells Can Form Kinapses in Lymph Nodes. Previous studies have shown that after a period of stable interaction with Ag-bearing DCs, T cells regain motility, adopt a swarming behavior, and establish mostly dynamic contacts with DCs (35, 36). The decrease in Ag load and the increase in responding T cells occurring in the late phase of T cell activation have been shown to contribute to the progressive loss of stable T cell–DC interactions (37). However, it is also possible that recently activated T cells establish more dynamic contacts than their naïve counterpart when facing an equivalent antigenic stimulus. To test this idea, we compared the behavior of naïve and recently activated T cells in the lymph node upon systemic administration of LPS and peptide. Naïve CD4$^+$ T cells bearing the LACK-specific WT15 T cell receptor (TCR), or the same T cells subjected to a short (3 days) in vitro stimulation with anti-CD3/CD28 beads, were labeled with carboxyfluorescein succinimidyl ester (CFSE) and adoptively

Author contributions: G.A.A. and P.B. designed research; G.A.A. and F.L. performed research; F.L. and E.A.R. contributed new reagents/analytic tools; G.A.A. and P.B. analyzed data; and P.B. wrote the paper.

The authors declare no conflict of interest.

This article is a PNAS Direct Submission. M.L.D. is a guest editor invited by the Editorial Board.

[1]To whom correspondence should be addressed. E-mail: philippe.bousso@pasteur.fr.

This article contains supporting information online at www.pnas.org/cgi/content/full/0905901107/DCSupplemental.

transferred into BALB/c recipients. Both T cell pools expressed CD62L and could home to lymph nodes, with naïve T cells being slightly more effective than recently activated T cells (Fig. S1). After 24 h mice were injected with LPS and 6 h later with LACK peptide. Thirty minutes after peptide injection, intact lymph nodes were imaged by two-photon microscopy. As shown in Fig.1*A* and Movie S1, naïve T cells immediately arrested upon Ag recognition. In the same conditions, activated T cells decelerated but did not stop. Quantification of mean velocities and trajectories straightness confirmed that upon Ag recognition, activated T cells migrated more rapidly and were less constrained than naïve T cells (Fig. 1*B*).

Thus, in these settings, Ag recognition occurs while activated T cells maintain a low level of motility, a behavior reminiscent of that of T cell dynamic contacts (35, 36, 38) or kinapses (1) seen during the late phase of activation.

To demonstrate that TCR signaling occurs during the slow migration of activated T cells observed in the presence of Ag, we relied on two approaches. First, we took advantage of the fact that CD62L is shed from the T cell surface within minutes of Ag recognition (39). As shown in Fig. S2*A*, activated T cells displayed decreased levels of CD62L as early as 30 min after peptide injection. Peptide injection also resulted in decreased CD3 levels, providing additional evidence for TCR engagement. Second, we labeled activated T cells with the calcium-sensitive dye Indo-1 (40) and after adoptive transfer, imaged T cells in lymph node 30 min after peptide injection. Short calcium spikes could be detected in activated T cells (Fig. S2*B*), most often between two phases of motility. These observations strongly suggest that kinapses indeed resulted in TCR signaling. In sum, our results indicate that recently activated T cells may intrinsically favor the formation of kinapses with DCs, a feature that likely contributes to the phase of transient contacts seen in the late stage of priming.

Generation and Activation of T Cells Expressing a LAT-EGFP Fusion Protein. Next we sought to determine the molecular distribution associated with Ag recognition by activated T cells. To this end, we used the murine stem cell virus (MSCV) retroviral vector system to induce the expression of a fusion protein consisting of the LAT scaffold protein and the enhanced GFP (LAT-EGFP). LACK-specific $CD4^+$ T cells isolated from WT15 TCR transgenic (Tg) mice were activated in vitro using of anti-CD3/anti-CD28 beads and subjected to two rounds of spin infection. After this procedure, an average of 42.2% ± 4.6% (mean ± SEM) of WT15 T cells expressed the fusion protein (Fig. 2*A*). In vitro imaging of T cells infected with either GFP or LAT-EGFP confirmed that LAT-EGFP was localized to the plasma membrane and within intracytoplasmic compartments, as previously reported (Fig. 2*B*) (33). Both LAT-EGFP-expressing T cells and noninfected T cells responded efficiently upon restimulation with peptide in vitro (Fig. S3). To test whether Ag-experienced

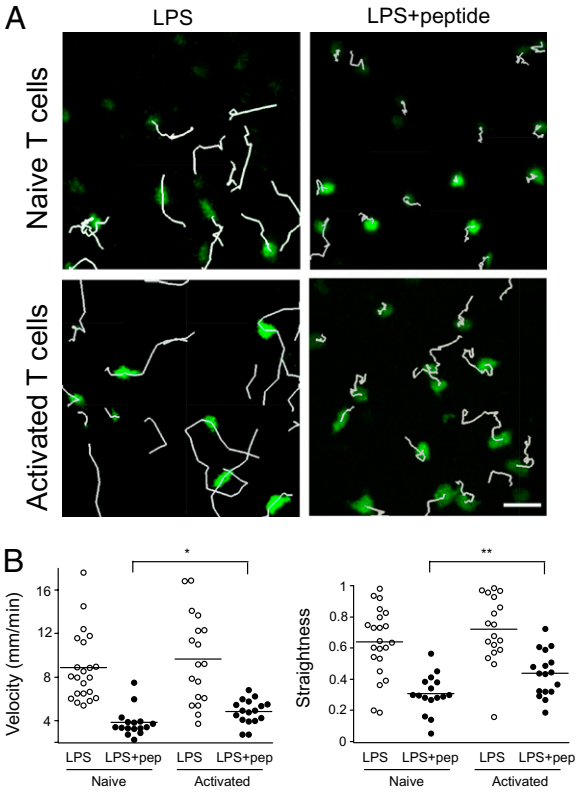

Fig. 1. Naïve and recently activated T cells display different behaviors during Ag recognition in the lymph node. Naive or in vitro activated $CD4^+$ T cells from WT15 TCR Tg mice were labeled with CFSE and adoptively transferred into BALB/c recipients. After 24 h, mice were injected with 50 μg LPS and 6 h later with 100 μg of LACK peptide. Control mice were injected with LPS only. Two-photon imaging of intact lymph nodes was performed 30 min after peptide injection. (*A*) Trajectories corresponding to 12 min of imaging are shown for naïve (*Top*) or activated T cells (*Bottom*) in response to LPS or LPS plus peptide. Naïve but not activated T cells completely arrested upon Ag recognition. (*B*) Quantitation of T cell velocities (*Left*) or straightness indexes (*Right*) in the different experimental conditions. Each dot represents an individual T cell. Low straightness indexes correspond to constrained behavior. $*P < 0.05$; $**P < 0.01$.

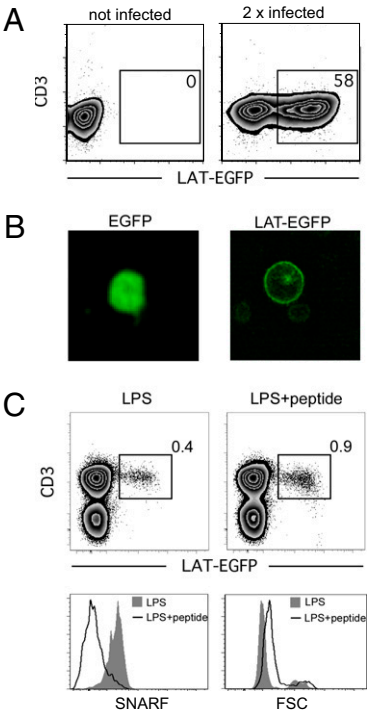

Fig. 2. Generation and in vivo response of LAT-EGFP-expressing T cells. $CD4^+$ T cells from WT15 TCR Tg mice were stimulated in vitro using anti-CD3/anti-CD28 coated beads and retrovirally transduced to express EGFP or LAT-EGFP. (*A*) LAT-EGFP expression by $CD4^+$ T cells was assessed by flow cytometry 24 h after transduction. (*B*) Imaging of T cells in suspension after infection with retroviral particles encoding EGFP or LAT-EGFP. (*C*) LAT-EGFP-expressing T cells divide in response to in vivo immunization. WT15 $CD4^+$ T cells were transduced to express LAT-EGFP, labeled with the SNARF dye, and adoptively transferred into BALB/c mice. Mice were injected with LPS and peptide or LPS alone. After 3 days, lymph nodes were harvested, and cells were stained with an anti-CD3 mAb. Flow cytometry shows that LAT-EGFP-expressing WT15 $CD4^+$ T cells increased in size and proliferated (as reflected by the dilution of SNARF intracellular content) in the presence but not in the absence of peptide.

LAT-EGFP-expressing T cells could also retain the ability to respond to antigenic stimulation in vivo, we labeled them with SNARF dye and adoptively transferred them into BALB/c recipients. Twenty-four hours later, mice were injected with LPS plus LACK peptide or LPS alone. As shown in Fig. 2*C*, LAT-EGFP-expressing T cells increased in size and proliferated (as evidenced by SNARF dilution) in the presence, but not in the absence, of the LACK peptide. Thus, this procedure allowed the generation of LAT-EGFP-expressing T cells capable of in vivo response to Ag stimulation.

Two-Photon Imaging of LAT-EGFP-Expressing T Cells in Intact Lymph Nodes. Previous two-photon imaging studies of T cell activation have relied on the brightness of fluorescent vital cytoplasmic dyes, such as CFSE or SNARF, or highly expressed fluorescent proteins, such as GFP (reviewed in ref. 41). The relatively strong fluorescent signal obtained in T cells expressing LAT-EGFP (Fig. 2*A*) prompted us to further investigate whether LAT-EGFP-expressing T cells could be visualized by two-photon imaging in intact lymph nodes. After retroviral transduction, WT15 $CD4^+$ T cells were labeled with SNARF dye and adoptively transferred. A representative three-dimensional reconstruction of an imaging volume within the T cell area is shown in Fig. 3 *A*–*C*. Both transduced ($SNARF^+GFP^+$) and nontransduced T cells ($SNARF^+GFP^-$) were detected in the T cell area at ratios corresponding to the efficiency of infection, indicating that LAT-EGFP expression did not alter T cell homing to lymph nodes. Individual T cells, with clearly identifiable membrane fluorescence, could be visualized up to 150 μm below the lymph node surface. When T cells were examined at higher magnification, LAT-EGFP fluorescence enabled the identification of subcellular structures that were not visible with SNARF labeling alone, including uropods and membrane protrusions (Fig. 3 *D* and *E*). In summary, our procedure allowed us to image LAT-EGFP distribution in individual T cells present in the T cell zone, illuminating subcellular structures missed when visualizing cells labeled with cytoplasmic dyes only.

Dynamics of LAT-EGFP Distribution in T Cells During the Formation of Immunological Kinapses in Lymph Nodes. Next we investigated the dynamics of LAT-EGFP distribution in T cells during two modes of Ag recognition in the lymph node. As a first model, we analyzed T cell responses to systemic administration of LPS plus peptide. WT15 $CD4^+$ T cells were retrovirally transduced to express LAT-EGFP, labeled with SNARF dye, and adoptively transferred into BALB/c recipients. With this strategy, both transduced (GFP^+SNARF^+) and nontransduced (GFP^-SNARF^+) T cells could be imaged simultaneously, allowing us to test whether LAT-EGFP expression alters T cell behavior. Mice were injected i.v. with 50 μg LPS and 6 h later with 100 μg of LACK peptide. Intact lymph nodes were typically imaged 30 min after peptide injection. In the absence of peptide (injection of LPS only), both transduced and nontransduced WT15 $CD4^+$ T cells migrated rapidly, with a mean velocity of 12.4 ± 0.6 μm/min and 11.6 ± 0.5 μm/min, respectively (Fig. 4 *A* and *B* and Movie S2). In the presence of peptide, WT15 T cells decelerated, with mean velocities dropping to 6.3 ± 0.6 μm/min for GFP^+ and to 7.1 ± 0.6 μm/min for GFP^- T cells. Importantly, the fact that GFP^+ and GFP^- cells displayed similar behavior confirms that infection with LAT-EGFP has no measurable effect on T cell dynamics in response to Ag (Fig. 4 *A* and *B* and Movie S2). Next, we imaged at higher magnification and examined the dynamics of LAT-EGFP in T cells. As shown in Fig. 4*C* and Movie S3, in the absence of Ag, LAT-EGFP was enriched at the uropod of fast-migrating T cells. Previous studies have reported that molecules such as CD2, CD43, and CD44 or GM-1-enriched domains are preferentially found in the uropod of migrating T cells, whereas chemokine receptors or GM-3 domains accumulate at the leading edge (42–45). Our observations provide further support for the segregation of leading-edge and uropod components in T cells migrating within a native tissue environment. In contrast, T cells that established kinapses in the presence of Ag and LPS lacked an evident uropod structure (Fig. 4*D* and Movie S4). LAT-EGFP fluorescence revealed that slowly moving T cells continuously extend membrane protrusions (Fig. 4*D* and Movie S4), a behavior that may reflect their ability to compare the level of TCR stimulation on neighboring APCs (46). In this respect, it is tempting to speculate that the presence of a high density of Ag-bearing APCs (as expected in this experimental setting) favors kinapse formation by allowing T cell to scan serial APCs. Finally, no persistent large-scale clustering of LAT-EGFP could be seen in the T cells in these settings (Fig. 4*D* and Movie S4). These results are consistent with the idea that transient interactions established by T cells with Ag-bearing APCs do not result in extensive molecular clustering at the contact zone. Because APCs could not be directly visualized in these experiments, we also imaged LAT-expressing T cells interacting with adoptively transferred peptide-pulsed DCs. As shown in Fig. S4 and Movie S5, most T cells were swarming around DCs, with no persistent large scale accumulation of LAT-EGFP fluorescence.

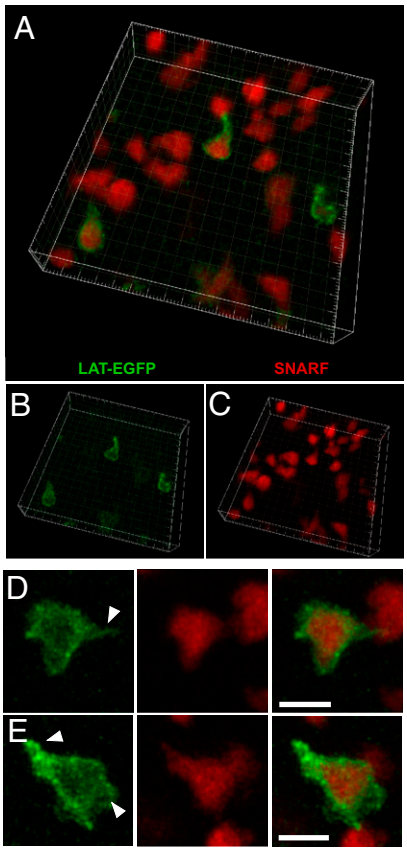

Fig. 3. Two-photon imaging of T cells expressing LAT-EGFP in intact lymph nodes. WT15 $CD4^+$T cells were transduced to express LAT-EGFP, labeled with SNARF dye, and transferred into BALB/c mice. Twenty-four hours after transfer, intact lymph nodes were subjected to two-photon imaging. (*A*–*C*) Three-dimensional reconstruction of an imaging volume within the T cell zone of the lymph node. Note that only a fraction of the T cells have been infected. GFP and SNARF signals are shown in *B* and *C*, respectively. Square side length = 5 μm. (*D* and *E*) Enlarged views of GFP and SNARF fluorescent signals for individual T cells. Note that GFP fluorescence allows for the detection of subcellular structures, including uropod and membrane protrusions that were not discernable with SNARF dye (white arrowheads). (Scale bar, 10 μm.)

Dynamics of LAT-EGFP Distribution in T Cells During the Formation of Immunological Synapses in Lymph Nodes. A previous study showed that in vitro, T cell–B cell but not T cell–DC conjugates displayed the hallmarks of mature synapses (15). Thus, as a second model of Ag

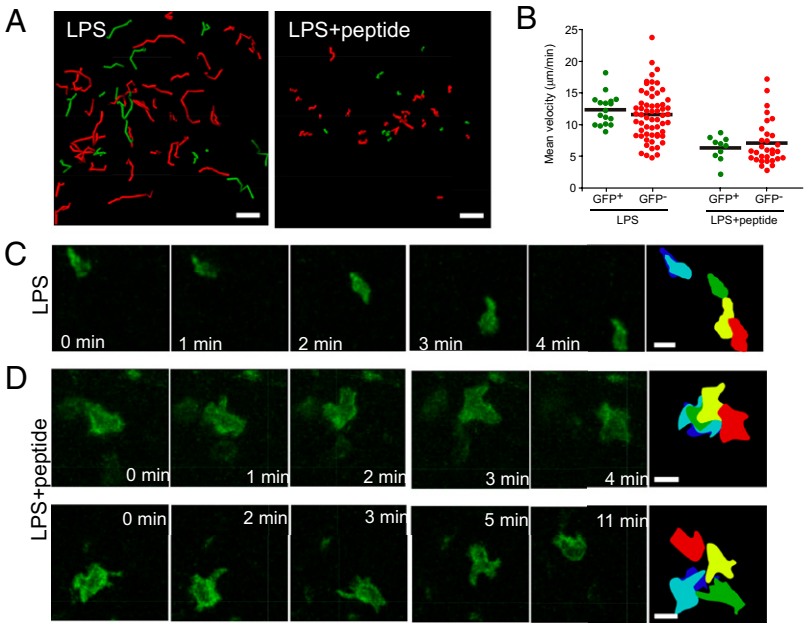

Fig. 4. Visualizing LAT-EGFP distribution in T cells during kinapses formation in lymph node. WT15 CD4$^+$ T cells were transduced to express LAT-EGFP, labeled with SNARF dye, and transferred into BALB/c mice. After 24 h, mice were injected with 50 μg LPS and 6 h later with 100 μg of LACK peptide. Control mice were injected with LPS only. Intact lymph nodes were subjected to two-photon imaging 1 h after peptide injection. (*A–C*) WT15 CD4$^+$ T cells decelerate but do not arrest in response to Ag. (Scale bar, 30 μm.) (*A*) Tracks of T cells (corresponding to 5 min of imaging) are shown for uninfected (GFP$^-$SNARF$^+$, red) and infected (GFP$^+$SNARF$^+$, green) WT15 CD4$^+$ T cells in mice injected with LPS or LPS and peptide. (*B*) Mean velocities of individual GFP$^+$ and GFP$^-$ WT15 CD4$^+$ T cells in response to LPS or LPS and peptide. (*C*) Zoomed-in time-lapse imaging of a representative LAT-EGFP-expressing WT15 CD4$^+$ T cell migrating vigorously in control mice (LPS only). Note that the T cell shape displays a typical elongated shape and that LAT-EGFP preferentially accumulates at the uropod. The last frame is a colored overlay of the T cell outlines at various time points. (Scale bar, 10 μm.) (*D*) Zoomed-in time-lapse imaging of two representative low-motile LAT-EGFP-expressing WT15 CD4$^+$ T cells in mice that received both LPS and LACK peptide. WT15 CD4$^+$ T cells sent out numerous and dynamic membranes protrusions, presumably while contacting host APCs. No stable accumulation of LAT-EGFP was evident during this process. Results are representative of three independent experiments. (Scale bar, 10 μm.)

recognition, we analyzed T cells interacting with peptide-pulsed B cells in intact lymph nodes. As expected from previous work (47–49), T cells appeared frequently conjugated to peptide-pulsed B cells but not to unpulsed B cells (Movie S6), and conjugated B cells remained motile and actively dragged the T cells. Importantly, we found that LAT-EGFP accumulated at the T cell–B cell interface (Fig. 5*A–F* and Movie S7), where the fluorescence intensity was 1.5–2 times higher than in the rest of the plasma membrane, and this enrichment was maintained over time (Fig. 5 *G* and *H*). Such accumulations could reflect recruitment of both the membrane and the intracellular pool of LAT as seen in vitro and/or membrane condensation at the interface. Although LAT-EGFP enrichment at the interface was evident in virtually all conjugates, the structure of the synapse was variable because one or several clusters of LAT-EGFP could be detected at the junction and were located at the center, at the periphery, or both. It is likely that our approach could not resolve smaller LAT clusters. In a few instances, we observed a T cell engaging two B cells simultaneously (Fig. 5*F* and Movie S8). In these cases LAT-EGFP was enriched at both contact zones. Interestingly, when one of the B cells detached, LAT-EGFP accumulation on the T cell was immediately and selectively lost at the corresponding site.

Conclusions

In the present study, we report two important findings. First, we demonstrate that the state of T cell activation and the type of APC strongly influence the dynamics of T cell–APC interactions in the lymph node. Previous studies have indicated that T cells form dynamic contacts with DCs in the late phases of priming. Although T cell competition and decrease in Ag load contribute to this phenomenon (37), our finding that activated T cells have a higher propensity to form kinapses than naïve T cells provides an additional mechanism for the progressive changes in contact dynamics during the course of T cell activation. In other circumstances, naïve T cells can also form kinapses (35, 50), suggesting that additional mechanisms influence kinapse vs. synapse formation.

Second, this study provides an initial link between two-photon imaging of T cell dynamics in the lymph node and molecular imaging of the immunological synapses in vitro. Although the present work has focused on previously activated T cells, future studies relying on retroviral infection of bone marrow cells should enable the study of naïve T cells as well (19). Visualizing LAT-EGFP distribution in T cells revealed at least three aspects of T cell biology that would not have been detected using conventional lymphocyte labeling with vital dyes or GFP. First, T cells migrating in the absence of Ag showed LAT-EGFP enrichment at the uropod, extending in vitro observation of molecules partitioning during migration (51). Second, T cells that slowly migrated during kinapse formation lacked a defined uropod but extended membrane protrusions with no persistent LAT-EGFP clustering. Finally, T cells establishing stable interactions with B cells in lymph nodes displayed durable enrichment of LAT-EGFP at the cell junction. The distinct dynamics of LAT-EGFP in T cells during activation highlight the plasticity of Ag recognition in secondary lymphoid tissues. The ability to visualize T cells with subcellular resolution in vivo will help clarify the relevance of some of the findings made with high-resolution in vitro imaging and broaden our understanding of T cell activation under physiologic settings.

Materials and Methods

Mice. BALB/c mice were purchased from Charles River. WT15 αβTCR transgenic BALB/c mice (52) were bred in our animal facility. This TCR recognizes an immunodominant epitope from the *Leishmania major* LACK protein in the

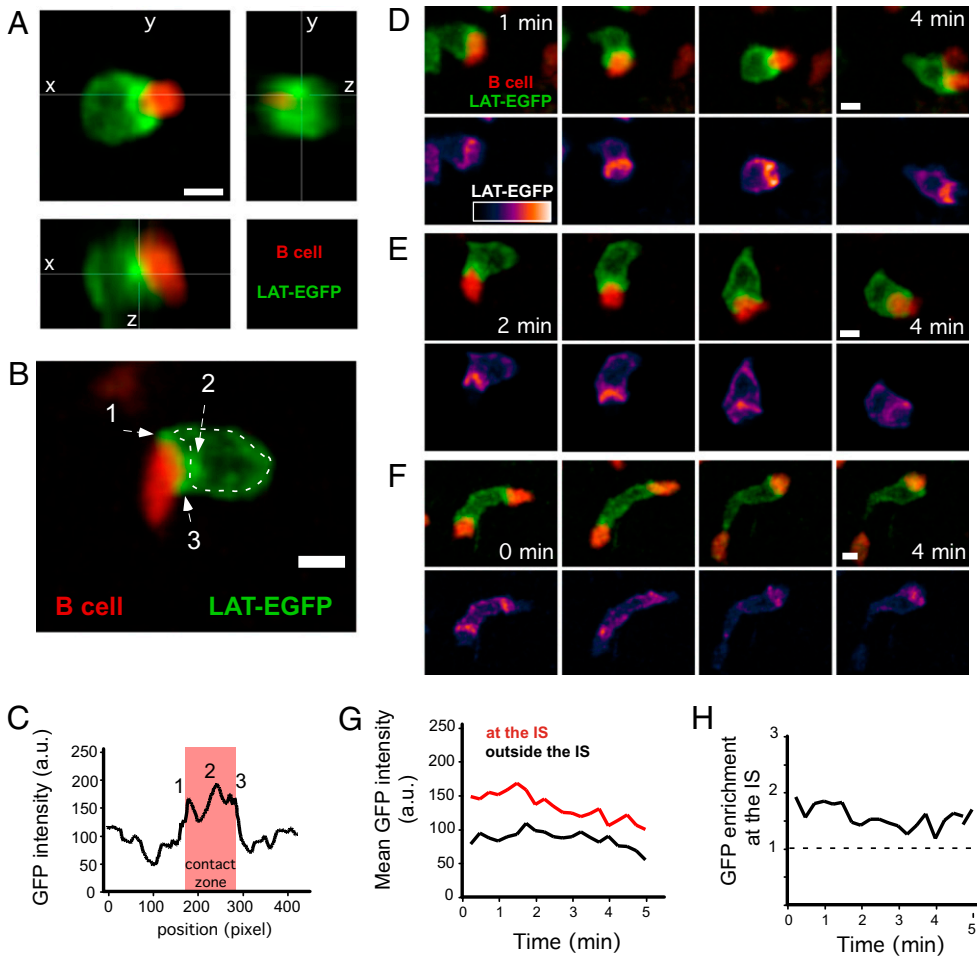

Fig. 5. Dynamics of LAT-EGFP in T cells forming stable immunological synapses with B cells in lymph nodes. WT15 CD4$^+$ T cells were transduced to express LAT-EGFP and adoptively transferred into BALB/c mice. After 24 h, SNARF-labeled peptide-pulsed B cells were transferred, and two-photon imaging of lymph nodes was performed 6 h later. (*A*) 3D reconstruction of a representative T cell–B cell conjugate showing LAT-EGFP fluorescence accumulation at the cell interface. Scale bar = 5 μm. (*B*) LAT-EGFP fluorescence accumulate at the T cell–B cell interface in distinct clusters (arrows). (*C*) The intensity of GFP fluorescence was graphed along the outline shown in *B* (a.u, arbitrary units). (*D* and *E*) Time-lapse imaging of two representative T cell–B cell immunological synapses. Scale bar = 5 μm. (*F*) Example of a T cell establishing two immunological synapses simultaneously. LAT-EGFP accumulated at both sites of interaction until one of the B cells detaches. (*G* and *H*) Quantitation of the mean LAT-EGFP fluorescence at immunological synapse or in the rest of the T cell surface showed a sustained enrichment at the contact zone. Results are shown for a representative T cell–B cell pair. Representative of at least 10 time-lapse movies obtained in two independent experiments. (Scale bars, 5 μm.)

context of I-A^d. All animal experiments were performed according to institutional guidelines for animal care and use.

Generation of LAT-EGFP-Expressing T Cells. LAT cDNA was amplified by PCR using the following primers: 5′ GA AGA TCT ATG GAA GCA GAC GCC TTG AGC and 3′ CGC GGA TCC GTT AAG CTC CTG TAG ATT. *Bgl*II-*BamH*I digestion product was cloned into a pMSCV 2.2-EGFP vector. The resulting LAT-EGFP construct was verified by sequencing. PlatE packaging cells (53) were transfected with pMSCV2.2-EGFP or pMSCV2.2-LAT-EGFP vectors by using Lipofectamin 2000 (Invitrogen) in OptiMEM for 6 h. Subsequently, packaging cells were maintained in RPMI supplemented by 10% FBS. After 48 h, cell supernatants were collected and used for T cell spin-infection. LACK-specific WT15 CD4$^+$ T cells were isolated by magnetic depletion (Miltenyi Biotec) from the spleens of WT15 TCR Tg animals. CD4$^+$ T cells were activated using anti-CD3/anti-CD28 activating beads (Dynal, Invitrogen) at 4:1 bead/cell ratio in the presence of 25 U/mL of recombinant IL-2. At 24 h and 48 h, T cells were resuspended in supernatant from transfected PlatE packaging cells in the presence of 8 μg/mL of polybrene (Sigma-Aldrich) and were centrifuged (1,200 × *g*) for 1 h at 32 °C. On day 3, beads were detached by gentle pipetting and removed magnetically. When indicated, T cells were labeled with 5 μM SNARF or CFSE (Invitrogen) for 10 min at 37 °C. Adoptive transfer was performed by i.v. injection of 5–10 × 10^6 T cells in recipient BALB/c mice. For calcium imaging, 50 × 10^6 T cells were labeled with 2 μM Indo-1 (Invitrogen) and adoptively transferred into recipient mice.

In Vivo T Cell Stimulation. BALB/c recipients were adoptively transferred with LAT-EGFP-transduced T cells. After 24 h, mice were injected i.v. with 50 μg of ultrapure *Escherichia coli* LPS (Invivogen) and 6 h later with 100 μg of LACK peptide (FSPSLEHPIVVSGSWD) (NeoMPS). To study T cell–B cell interactions, BALB/c recipients were adoptively transferred with LAT-EGFP-transduced T cells and 24 h later with 10 × 10^6 peptide-pulsed B cells. B cells were magnetically isolated from spleens of BALB/c mice using anti-CD19 microbeads (Miltenyi Biotec), stained with 5 μM SNARF dye, and pulsed with 1 μM of LACK peptide for 30 min at RT. Splenic DCs were purified using CD11c microbeads (Miltenyi Biotec), labeled with 5 μM SNARF, and pulsed with 1 μM of LACK peptide.

Two-Photon Imaging. Two-photon imaging was performed using an upright microscope DM 6000B with an SP5 confocal head (Leica Microsystems). Explanted lymph nodes were maintained at 37 °C and perfused with media bubbled with a 95% O_2/5% CO_2 gas mixture. Samples were excited with a Chameleon Ultra Ti:Sapphire laser (Coherent) tuned at 950 nm, and emitted fluorescence was collected with nondescanned detectors. Typically, 12 z-planes spaced 1 to 2 μm apart were imaged every 15 s. For calcium imaging, the laser was tuned at 740 nm, and emitted fluorescence was split with a 440-nm dichroic mirror and a 525/50 band-pass filter. Upon calcium elevation, T cells appeared pseudocolored in green. Three-dimensional cell tracking was performed using Imaris software (Bitplane). Movies were processed using ImageJ and Imaris.

ACKNOWLEDGMENTS. We thank A. Alcover and members of the Bousso laboratory for comments on the manuscript. This work was supported by Institut Pasteur, Institut National de la Santé et de la Recherche Médicale, Mairie de Paris, and a Marie Curie Excellence Grant.

1. Dustin ML (2008) Hunter to gatherer and back: Immunological synapses and kinapses as variations on the theme of amoeboid locomotion. *Annu Rev Cell Dev Biol* 24: 577–596.
2. Billadeau DD, Nolz JC, Gomez TS (2007) Regulation of T-cell activation by the cytoskeleton. *Nat Rev Immunol* 7:131–143.
3. Das V, et al. (2002) Membrane-cytoskeleton interactions during the formation of the immunological synapse and subsequent T-cell activation. *Immunol Rev* 189:123–135.
4. Geiger B, Rosen D, Berke G (1982) Spatial relationships of microtubule-organizing centers and the contact area of cytotoxic T lymphocytes and target cells. *J Cell Biol* 95: 137–143.
5. Kupfer A, Dennert G (1984) Reorientation of the microtubule-organizing center and the Golgi apparatus in cloned cytotoxic lymphocytes triggered by binding to lysable target cells. *J Immunol* 133:2762–2766.
6. Monks CR, Freiberg BA, Kupfer H, Sciaky N, Kupfer A (1998) Three-dimensional segregation of supramolecular activation clusters in T cells. *Nature* 395:82–86.
7. Grakoui A, et al. (1999) The immunological synapse: A molecular machine controlling T cell activation. *Science* 285:221–227.
8. Gaus K, Chklovskaia E, Fazekas de St Groth B, Jessup W, Harder T (2005) Condensation of the plasma membrane at the site of T lymphocyte activation. *J Cell Biol* 171: 121–131.
9. Krummel MF, Sjaastad MD, Wülfing C, Davis MM (2000) Differential clustering of CD4 and CD3zeta during T cell recognition. *Science* 289:1349–1352.
10. Bunnell SC, et al. (2002) T cell receptor ligation induces the formation of dynamically regulated signaling assemblies. *J Cell Biol* 158:1263–1275.
11. Campi G, Varma R, Dustin ML (2005) Actin and agonist MHC-peptide complex-dependent T cell receptor microclusters as scaffolds for signaling. *J Exp Med* 202:1031–1036.
12. Yokosuka T, et al. (2005) Newly generated T cell receptor microclusters initiate and sustain T cell activation by recruitment of Zap70 and SLP-76. *Nat Immunol* 6:1253–1262.
13. Douglass AD, Vale RD (2005) Single-molecule microscopy reveals plasma membrane microdomains created by protein-protein networks that exclude or trap signaling molecules in T cells. *Cell* 121:937–950.
14. Trautmann A, Valitutti S (2003) The diversity of immunological synapses. *Curr Opin Immunol* 15:249–254.
15. Reichardt P, et al. (2007) Naive B cells generate regulatory T cells in the presence of a mature immunologic synapse. *Blood* 110:1519–1529.
16. Singleton KL, et al. (2009) Spatiotemporal patterning during T cell activation is highly diverse. *Sci Signal* 2:ra15.
17. Brossard C, et al. (2005) Multifocal structure of the T cell - dendritic cell synapse. *Eur J Immunol* 35:1741–1753.
18. Hailman E, Burack WR, Shaw AS, Dustin ML, Allen PM (2002) Immature CD4(+)CD8(+) thymocytes form a multifocal immunological synapse with sustained tyrosine phosphorylation. *Immunity* 16:839–848.
19. Stoll S, Delon J, Brotz TM, Germain RN (2002) Dynamic imaging of T cell-dendritic cell interactions in lymph nodes. *Science* 296:1873–1876.
20. Barcia C, et al. (2006) In vivo mature immunological synapses forming SMACs mediate clearance of virally infected astrocytes from the brain. *J Exp Med* 203:2095–2107.
21. Reichert P, Reinhardt RL, Ingulli E, Jenkins MK (2001) Cutting edge: In vivo identification of TCR redistribution and polarized IL-2 production by naive CD4 T cells. *J Immunol* 166: 4278–4281.
22. McGavern DB, Christen U, Oldstone MB (2002) Molecular anatomy of antigen-specific CD8(+) T cell engagement and synapse formation in vivo. *Nat Immunol* 3:918–925.
23. Khanna KM, McNamara JT, Lefrançois L (2007) In situ imaging of the endogenous CD8 T cell response to infection. *Science* 318:116–120.
24. Miller MJ, Wei SH, Parker I, Cahalan MD (2002) Two-photon imaging of lymphocyte motility and antigen response in intact lymph node. *Science* 296:1869–1873.
25. Lin J, Miller MJ, Shaw AS (2005) The c-SMAC: Sorting it all out (or in). *J Cell Biol* 170: 177–182.
26. Cahalan MD, Parker I (2008) Choreography of cell motility and interaction dynamics imaged by two-photon microscopy in lymphoid organs. *Annu Rev Immunol* 26: 585–626.
27. Bousso P (2008) T-cell activation by dendritic cells in the lymph node: Lessons from the movies. *Nat Rev Immunol* 8:675–684.
28. Cahalan MD, Parker I (2005) Close encounters of the first and second kind: T-DC and T-B interactions in the lymph node. *Semin Immunol* 17:442–451.
29. Dustin ML (2008) T-cell activation through immunological synapses and kinapses. *Immunol Rev* 221:77–89.
30. Zhang W, Sloan-Lancaster J, Kitchen J, Trible RP, Samelson LE (1998) LAT: The ZAP-70 tyrosine kinase substrate that links T cell receptor to cellular activation. *Cell* 92:83–92.
31. Zhang W, Trible RP, Samelson LE (1998) LAT palmitoylation: Its essential role in membrane microdomain targeting and tyrosine phosphorylation during T cell activation. *Immunity* 9: 239–246.
32. Shogomori H, et al. (2005) Palmitoylation and intracellular domain interactions both contribute to raft targeting of linker for activation of T cells. *J Biol Chem* 280:18931–18942.
33. Bonello G, et al. (2004) Dynamic recruitment of the adaptor protein LAT: LAT exists in two distinct intracellular pools and controls its own recruitment. *J Cell Sci* 117:1009–1016.
34. Houtman JC, et al. (2006) Oligomerization of signaling complexes by the multipoint binding of GRB2 to both LAT and SOS1. *Nat Struct Mol Biol* 13:798–805.
35. Mempel TR, Henrickson SE, Von Andrian UH (2004) T-cell priming by dendritic cells in lymph nodes occurs in three distinct phases. *Nature* 427:154–159.
36. Miller MJ, Safrina O, Parker I, Cahalan MD (2004) Imaging the single cell dynamics of CD4+ T cell activation by dendritic cells in lymph nodes. *J Exp Med* 200:847–856.
37. Garcia Z, et al. (2007) Competition for antigen determines the stability of T cell-dendritic cell interactions during clonal expansion. *Proc Natl Acad Sci USA* 104:4553–4558.
38. Hugues S, et al. (2004) Distinct T cell dynamics in lymph nodes during the induction of tolerance and immunity. *Nat Immunol* 5:1235–1242.
39. Sinclair LV, et al. (2008) Phosphatidylinositol-3-OH kinase and nutrient-sensing mTOR pathways control T lymphocyte trafficking. *Nat Immunol* 9:513–521.
40. Wei SH, et al. (2007) Ca2+ signals in CD4+ T cells during early contacts with antigen-bearing dendritic cells in lymph node. *J Immunol* 179:1586–1594.
41. Celli S, Garcia Z, Beuneu H, Bousso P (2008) Decoding the dynamics of T cell-dendritic cell interactions in vivo. *Immunol Rev* 221:182–187.
42. Tibaldi EV, Salgia R, Reinherz EL (2002) CD2 molecules redistribute to the uropod during T cell scanning: Implications for cellular activation and immune surveillance. *Proc Natl Acad Sci USA* 99:7582–7587.
43. Gómez-Móuton C, et al. (2001) Segregation of leading-edge and uropod components into specific lipid rafts during T cell polarization. *Proc Natl Acad Sci USA* 98: 9642–9647.
44. Friedl P, Entschladen F, Conrad C, Niggemann B, Zänker KS (1998) CD4+ T lymphocytes migrating in three-dimensional collagen lattices lack focal adhesions and utilize beta1 integrin-independent strategies for polarization, interaction with collagen fibers and locomotion. *Eur J Immunol* 28:2331–2343.
45. Nieto M, et al. (1997) Polarization of chemokine receptors to the leading edge during lymphocyte chemotaxis. *J Exp Med* 186:153–158.
46. Faroudi M, et al. (2003) Lytic versus stimulatory synapse in cytotoxic T lymphocyte/target cell interaction: manifestation of a dual activation threshold. *Proc Natl Acad Sci USA* 100:14145–14150.
47. Okada T, et al. (2005) Antigen-engaged B cells undergo chemotaxis toward the T zone and form motile conjugates with helper T cells. *PLoS Biol* 3:e150.
48. Gunzer M, et al. (2004) A spectrum of biophysical interaction modes between T cells and different antigen-presenting cells during priming in 3-D collagen and in vivo. *Blood* 104:2801–2809.
49. Qi H, Cannons JL, Klauschen F, Schwartzberg PL, Germain RN (2008) SAP-controlled T-B cell interactions underlie germinal centre formation. *Nature* 455:764–769.
50. Sims TN, et al. (2007) Opposing effects of PKCtheta and WASp on symmetry breaking and relocation of the immunological synapse. *Cell* 129:773–785.
51. Friedl P, Weigelin B (2008) Interstitial leukocyte migration and immune function. *Nat Immunol* 9:960–969.
52. Wang Q, et al. (2001) CD4 promotes breadth in the TCR repertoire. *J Immunol* 167: 4311–4320.
53. Morita S, Kojima T, Kitamura T (2000) Plat-E: An efficient and stable system for transient packaging of retroviruses. *Gene Ther* 7:1063–1066.